Deciphering Sb Sources and Transport Processes in a Mining and Smelting-Impacted River System (Oruro, Bolivia): Insights from Sb Isotopes

Colin Ferrari, Eléonore Resongles, Rémi Freydier, Marizol Flores, Mauricio Ormachea, Gerardo Zamora Echenique, Corinne Casiot

Deciphering Sb sources and transport processes in a mining and smelting-impacted river system (Oruro, Bolivia): insights from Sb isotopes.

Colin Ferrari[a], Eléonore Resongles[a,b*], Rémi Freydier[a], Marizol Flores[a,b], Mauricio Ormachea[b], Gerardo Zamora Echenique[c] and Corinne Casiot[a]

[a]HydroSciences Montpellier, Université de Montpellier, CNRS, IRD, Montpellier, France

[b]Instituto de Investigaciones Químicas, Universidad Mayor de San Andrés, Ciudad Universitaria, Calle 27 de Cota, La Paz, Bolivia

[c]Universidad Técnica de Oruro, Oruro, Bolivia

*corresponding author

Mailing address: Université Montpellier – HydroSciences
Bâtiment HYDROPOLIS
15 avenue Charles Flahault
34090 Montpellier, FRANCE
Email: eleonore.resongles@ird.fr

Abstract

Antimony (Sb) is a contaminant of increasing concern; its sources and fate in the environment require particular attention and its isotopes could be useful geochemical tracers. In this study, Sb isotopic composition was investigated along two rivers impacted by mining and smelting activities in the city of Oruro (Bolivia). Antimony concentration and isotope ratio were measured in water, suspended particulate matter and sediments during two contrasted seasons along a gradient of pH (from 1.6 to 6.5) and Sb concentration (from 8057 to 7 $\mu g.L^{-1}$). Antimony isotopic composition varied over a range of ~1 ‰ considering all sample types ($-0.09 \leq \delta^{123}Sb \leq +0.93$ ‰). The main stream impacted by acid mine drainage showed a progressive increase of $\delta^{123}Sb$ in the dissolved phase (+0.42 to +0.70 ‰), concomitant to Fe precipitation and Sb concentration decrease. This suggested that natural Sb attenuation by sorption onto neoformed Fe oxyhydroxysulphates was involved as this process favours light isotopes in the solid ($\Delta^{123}Sb_{water\text{-}sediments}$ averaged +0.3 ‰). Smelting-impacted tributary exhibited lighter dissolved Sb ($+0.29 \leq \delta^{123}Sb \leq +0.36$ ‰). Lake Uru-Uru which receives both rivers exhibited a $\delta^{123}Sb$ value of +0.28 ‰ in the wet season and +0.55 ‰ in the dry season, which might reflect different contributions of the AMD- and smelter-impacted rivers. The study reveals, for the first time, the impact of two distinct anthropogenic sources on antimony (Sb) isotopic composition on a water body and provides new insights into the ability of antimony isotopes to trace sources and processes in contaminated aquatic systems.

Keywords

Antimony isotopes; antimony isotope fractionation; mining and metallurgy pollution; river contamination; mining waters; mine wastes.

1. Introduction

Antimony (Sb) is a toxic metalloid critical to modern and emerging technologies (Dembele *et al.,* 2022). Antimony is mainly used in plastics as a flame retardant or catalyst (for PET), in batteries and lead alloys as a hardener, in brake linings as a lubricant, in glass as a decolouring agent and in semiconductors as a modulator of electrical properties (Dembele *et al.,* 2022). With the intensification of its extraction and industrial applications, Sb has become an emerging environmental contaminant of significant concern (Bolan *et al.*, 2022; Fu *et al.*, 2023). The environments most affected by antimony contamination are in areas impacted by sulphide mining and smelting activities (He *et al.*, 2019; Bolan *et al.*, 2022; Fu *et al.*, 2023). For instance, surface waters and groundwaters of the Xikuangshan antimony mining and smelting area in China suffer from severe Sb contaminations, with dissolved Sb concentrations exceeding background levels in pristine rivers (typically <1 µg/L) by up to three orders of magnitude (Guo *et al.*, 2018; Wen *et al.*, 2023). These environmental contaminations pose a health risk to neighbouring ecosystems and human populations. Indeed, despite limited studies, Sb is deemed toxic to organisms and humans, some Sb compounds being classified as potential human carcinogens (Sundar and Chakravarty, 2010; Bolan *et al.*, 2022; Fu *et al.*, 2023). In humans, while antimony toxicity has been demonstrated in the context of occupational exposure (Cavallo *et al.*, 2002; Saerens *et al.*, 2019), little information exists on the health effects of an environmental exposure at lower levels. Findings from the NHANES cohort study in the USA general population indicated that individuals with elevated Sb urine concentrations statistically showed a higher prevalence of cardiovascular diseases compared to the rest of the population, suggesting that environmental exposure to Sb represents a health hazard in the general population (Guo *et al.*, 2016). The exposure routes to Sb can include ingestion and inhalation of contaminated particles such as mining dust, industrial emissions and urban dust (Barbieri *et al.*, 2011, 2014; Fort *et al.*, 2016) and consumption of contaminated drinking water or food (Ye *et al.*, 2018; He *et al.*, 2019).

The primary process of antimony release to the aquatic compartment around sulphide mining sites is the dissolution of stibnite (Sb_2S_3), the main Sb ore, and other Sb-rich sulphides and sulfosalts (e.g., tetrahedrite $(Cu,Fe)_{12}Sb_4S_{13}$, boulangerite $Pb_5Sb_4S_{11}$, bournonite $CuPbSbS_3$ jamesonite $Pb_4FeSb_6S_{14}$, zinkenite $Pb_9Sb_{22}S_{42}$) (Zhou *et al.*, 2017; He *et al.*, 2019; Hao *et al.*, 2021; Fu *et al.*, 2023, Kaufmann *et al*., 2023). Depending on the nature of ore mineralisation and host rocks, the generation of acid mine drainage (AMD) originating from the oxidation of sulphide minerals in contact with water and oxygen can occur. AMD is characterized by acid leachates that may contain hundreds micrograms per litre to several milligrams per litre of antimony (Filella *et al.*, 2009; Ritchie *et al.*, 2013; Resongles et al., 2013; Chen *et al.*, 2023). The fate of Sb in sulphide-mining environments and downstream hydrosystems involves complex (bio-)geochemical processes including redox changes (from Sb(+III) to

Sb(+V)), sorption on neoformed iron oxyhydroxides and oxyhydroxysulphates or precipitation of secondary Sb minerals (Filella *et al.*, 2009; Resongles *et al.*, 2013; He *et al.*, 2019; Bolan *et al.*, 2022). Smelters or other metallurgical industries are other sources of Sb to the aquatic environment; this element is enriched in rivers around smelters as a result of rainwater leaching of contaminated atmospheric dust and soils, effluent discharge or slag leaching and erosion (Wilson *et al.,* 2004; Wang *et al.*, 2011; Goix *et al.*, 2013; Liao *et al.*, 2023).

Antimony stable isotope geochemistry (^{121}Sb and ^{123}Sb isotopes with average abundances of 57.213 % and 42.787 % (Chang *et al.*, 1993)) is not well characterized yet but it has attracted a growing interest in recent years in various fields including archaeometallurgy, metallogeny or environmental sciences (Resongles *et al.*, 2015; Degryse *et al.*, 2020; Kaufmann *et al.*, 2023 and references therein). The main Sb ore, stibnite (Sb_2S_3), exhibits a significant range of Sb isotopic composition (δ^{123}Sb) around 1 ‰, including within a single deposit which may be explained by kinetic and/or redox-induced Sb isotopic fractionation during the precipitation of stibnite from the hydrothermal fluid (Wang *et al.*, 2021; Zhai *et al.*, 2021; Kaufmann *et al.*, 2023). Recent studies have investigated Sb isotope signatures in the environment, they revealed the potential of Sb isotopes as tracers of Sb sources and/or biogeochemical processes (Resongles *et al.*, 2015; Liao *et al.*, 2023; Philippe *et al.*, 2023; Wen *et al.*, 2023; Guillevic *et al.*, 2024; Kaufmann e*t al.*, 2024; Liu *et al.*, 2024; Wu *et al.*, 2024; Wu *et al.*, 2025). In river systems impacted by historic metal and Sb mines, Resongles *et al.*, (2015) used the δ^{123}Sb signature to determine the contribution of two sub-watersheds to the total dissolved Sb load. More recently, Wen *et al.* (2023) investigated changes in Sb isotope signature in mine waters, river waters and groundwaters in the area of the Xikuangshan mine. Mine waters showed a wide range of Sb isotopic composition (-0.20 ‰ < δ^{123}Sb < +0.37 ‰) generated by a combination of processes (stibnite oxidative dissolution, Sb adsorption on Fe/Mn (hydr)oxides and mixing) while downstream, the impacted river water had a steady signature suggesting a conservative transport of Sb in the dissolved phase (Wen *et al.*, 2023) and in river sediments (Liu et al., 2024). In addition, no large isotopic fractionation (δ^{123}Sb = 0.29 ± 0.14 ‰) was observed among Sb ore, slag and dust samples from a modern Sb smelter site indicating that the high-temperature industrial process did not fractionate Sb isotopes (Liao *et al.,* 2023) unlike previously observed for other metal isotopes such as Cd or Zn (Sivry *et al.*, 2008; Sonke *et al.*, 2008; Gao *et al.*, 2013) and for Sb at an old Pb smelting site (Guillevic *et al.*, 2024). These contradictory findings suggest that Sb fractionation associated with smelting may depend on the technology involved. Large Sb isotopic fractionation (0.23 ‰ < δ^{123}Sb < 1.19 ‰) was observed in soil profiles affected by smelting emissions; it was ascribed to post-depositional biogeochemical processes (plant uptake, adsorption and reductive dissolution, Liao *et al.*, 2023). Overall, a comprehensive knowledge is lacking about the direction and amplitude of isotopic fractionation

generated by biogeochemical processes in mining waters. Recent studies investigated the fractionation of Sb isotopes associated with Sb sorption on Al-oxides, Mn-oxides or Fe-oxyhydroxides showing either no isotopic fractionation (Al-oxides) or an enrichment with the light isotope in the adsorbed phase (Fe oxy(hydro)xides, Mn-oxides) (Zhou *et al.*, 2022; Zhou *et al.*, 2023; Luo *et al.,* 2024; Ferrari *et al.*, 2024; Wen et al., 2024; Zhou et al., 2024), the latter was further confirmed with field observations along a basaltic weathering profile (Wu *et al.*, 2024). The abiotic reduction of Sb(V) into Sb(III) by different reducing agents (potassium iodide, sulphide) produced enrichment in the lighter isotope by -0.5 to -1.4 ‰ in the reduced species (Rouxel *et al.,* 2003; Veldhuizen *et al.*, 2023), in agreement with the result of theoretical Sb isotope fractionation calculations regarding Sb(III) oxides vs Sb(V) oxides (Ferrari *et al.*, 2022). On the other hand, biotic oxidation of Sb(III) to Sb(V) by two different Sb tolerant bacterial strains isolated from a Sb-rich mine drainage in France *(Ensifer sp.)* and a soil in a Sb mining area in China *(Pseudomonas sp.* J1*)*, resulted in a fractionation factor $\Delta^{123}Sb_{Sb(V)-Sb(III)}$ of about -0.20 ‰ *(Ensifer sp.)* and -0.60 ‰ (*Pseudomonas sp.* J1), in relation with a kinetic effect (Ferrari *et al.*, 2023; Jia et al., 2024). Altogether, these pioneer results suggest that Sb isotopes could contribute to identifying the sources and processes affecting Sb mobility in environments impacted by both mining and smelting activities, although it has never been attempted to date.

The aim of this study was to explore the potential of antimony isotopes as an environmental tracer for identifying Sb sources and/or tracking Sb transport processes in complex aquatic environments impacted both by mining and smelting activities. For this, the mining and industrial town of Oruro (~265 000 inhabitants) in Bolivia, the 5th largest Sb producer worldwide, was chosen as the study site. Indeed, Oruro represented an ideal case-study since it suffers severe Sb contamination of surface waters, soils and atmospheric particles originating from multiple Sb sources, i.e. different mining and smelting sites (Goix, 2012), and human exposure to Sb was proven (Barbieri *et al.*, 2016). The fate of Sb isotopes was investigated along two river systems impacted by acid mine drainage and smelter effluents in this area, during two contrasted hydrological periods. Antimony concentrations and isotopic compositions were determined in the dissolved phase, suspended particulate matter and sediment, together with aqueous Sb speciation, in order to identify the processes involved. The specific objectives of the study were i) to document the range of Sb isotope signatures, in relation to the multiple sources and geochemical processes at work, that may imprint significant spatial and temporal change in Sb isotope signature and ii) to interpret these changes in the light of recent results from theoretical and experimental studies that documented Sb isotopic fractionation factors associated with adsorption processes and redox changes. One expected outcome was evaluating the relevance of the application of Sb isotopes as source and/or process tracers in complex aquatic environments impacted by multiple mining and industrial sources.

2. Materials & methods

2.1 Study area

Bolivia is the 5th largest Sb producer after China, Russia, Tajikistan, Burma and Australia, with a production of 2500-3100 tons of Sb per year (2018-2022 data, U.S.G.S., 2023). Oruro is the largest mining city (264 643 inhabitants in 2012) in the Bolivian Altiplano located within the Bolivian Tin Belt in the Cordillera Oriental, 230 km southeast of La Paz, at an altitude of 3700-4200 m above sea level. The climate is characterised by two seasons, the dry season, from May to October and the wet season, from December to March, with a precipitation average of 375 mm annually.

The Sb-rich silver-tin deposit, exploited for over 400 years, and the largest local mine of San José are located in dacitic and rhyolitic volcanic rocks from the Tertiary on the western side of the city of Oruro (Figure 1). This volcanic dome (Oruro complex) is embedded in Silurian rocks (mainly sandstones and siltstones) that outcrop in the mountainous area to the east of Oruro (Gomez et al., 2019). Within the Oruro city area, the Silurian bedrock is covered by unconsolidated fluvial-lacustrine Quaternary sediments from tenths to hundreds of meters, mainly composed by quartz and other silicates and which forms a porous aquifer used for drinking water supply (Gomez et al., 2019).

Within the Oruro volcanic complex, besides Ag and Sn minerals, the sulfidic ores also contain antimony and other base metals and metalloids (e.g., As, Pb, Zn). Antimony is associated with many Sb-rich sulfosalts such as tetrahedrite ($(Cu,Fe)_{12}Sb_4S_{13}$), pyrargyrite (Ag_3SbS_3), boulangerite ($Pb_5Sb_4S_{11}$), andorite ($PbAgSb_3S_6$) and metastibnite (amorphous Sb_2S_3) (Keutsch and Brodtkorb, 2008). The exploitation of sulphide deposits produces acid mine drainage (AMD); the most important AMD effluent flows outside from the San José mine gallery entrance and joins the Rio Tagarete, forming the Canal Rosso (CR), which crosses the city and receives untreated urban wastewaters (Figure 1). The Canal Rosso joins Lake Uru-Uru to the south, after a 16 km course. Dissolved Sb concentration in this AMD was previously measured at 8080 ± 701 µg.L^{-1} at the exit of the mine gallery and a decrease was observed down to 19 ± 7 µg.L^{-1} about 10 km downstream (Goix, 2012). In the AMD at the exit of the mine gallery, the neo-formed minerals detected by XRD were mainly Ca, Fe and Al sulphates (such as gypsum ($CaSO_4{\cdot}2H_2O$), halotrichite ($FeAl_2(SO_4)_4{\cdot}22H_2O$), kalinite ($KAl(SO_4)_2{\cdot}11H_2O$) or rozenite ($FeSO_4{\cdot}4(H_2O)$) while primary sulphides (including Sb sulphides such as boulangerite and andorite) were also found (Goix, 2012). In addition, Fe oxy(hydro)xides (goethite, hematite and ferrihydrite) were present at the mine exit and further downstream in the AMD (Goix et al., 2012).

East of Oruro, in the city of Vinto, the largest Sn smelter in the country is responsible for a severe metal(loid) contamination in airborne particles (Goix *et al.*, 2016). Antimony concentrations in

surface waters draining the smelter complex were not determined previously but drinking water in the Vinto area showed high Sb levels, up to 49 µg.L^{-1} (Goix, 2012).

2.2 Sampling

2.2.1 Sampling sites

Two sampling campaigns were conducted, the first one at the end of the wet season, in March 2019 and the second one at the end of the dry season, in October 2021. During both campaigns, samples were collected at 10 stations (Figure 1): 1) five stations along the river continuum from the San Jose mine gallery exit to Lake Uru-Uru (stations SJ1, CR1, CR2, CR3 and LUU), 2) two stations along the river draining the Vinto smelter area (Vinto River, stations V1 and V2), 3) in another urban canal (station URB, sampled in 2021 only) and 4) two natural reference sites not impacted by AMD, urban, or smelting activities (stations CC and PAR, sampled in 2021 only). One reference site was located along the Cala-Cala River (station CC), upstream from the confluence with the river draining the Vinto smelter area; this site had been identified by Tapia *et al.*, (2012) to be representative of the geochemical background. A second reference site was located along the river Paria (station PAR), around 10 km NNE of the city of Oruro. A fourth sample set consisted of four drinking tap water samples; they were collected from the tap in the centre of Oruro and in east, centre, and south-west neighbourhoods of Vinto urban area. Water from Oruro's unified drinking water network originates mainly (at 85 %) from a nearby well field to the north of the city and from wells located between Oruro and Vinto urban areas (Gomez 2016; SELA, 2023), both well fields exploit the porous aquifer of Quaternary sediments. Vinto's drinking water supply network is separate from that of Oruro and it also exploits local wells in the porous Quaternary aquifer but groundwater flowpaths are disconnected from the Oruro well field (Gomez et al., 2016). A previous study showed high levels of Sb (10-49 µg.L^{-1}) in Vinto drinking water in 2007 suggesting a possible impact of the smelter on the quality of local groundwater, with variations depending on the neighbourhood, which prompted sampling in three different areas of Vinto in this study.

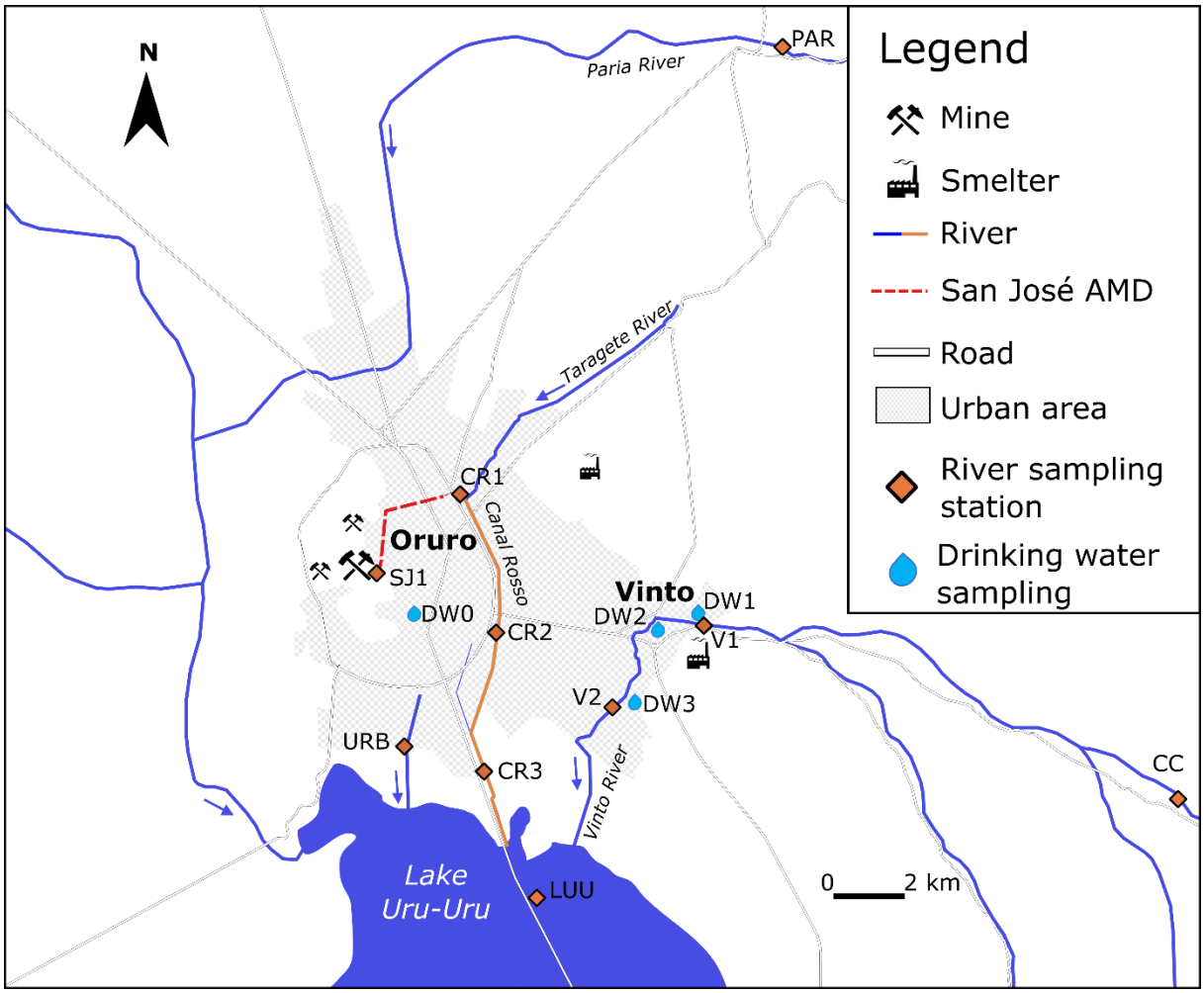

Figure 1: Location of the sampling stations and the main mining and metallurgical sites in the city of Oruro (Bolivia).

2.2.2 Sample collection and field measurements

The sampling in 2019 and 2021 included water (<0.22 µm) and riverbed sediment. In 2021, only dry sediments were collected at stations V1 and V2 due to river drying at these sites at the end of the dry season. Suspended particulate matter (SPM) was collected only in 2021. A summary of the samples and parameters taken at each station and at each season is given in Appendix (Table S1).

The pH, conductivity, redox potential and dissolved oxygen concentration (DO) were measured in the field using an HQ40D portable multi-meter (Hach®) during the 2021 campaign. Surface sediments were collected with a stainless-steel spatula in a plastic box and homogenised before being stored in a 30 mL PE vial and kept in a cool box until returned to the laboratory.

Water samples for dissolved organic carbon (DOC) analysis were filtrated in the field using a glass syringe (previously rinsed 3-times with ultrapure water and 3-times with sampled water) and a disposable 0.22 µm PVDF filter, the filtrate was collected in a decontaminated glass bottle and stabilised in 0.015 M H_3PO_4 (Suprapur, Merck®). 2 L of raw water were collected in an acid-cleaned HDPE bottle rinsed 3-times with the sampled water. A first subsample was immediately filtered *in situ*

using a disposable syringe and a 0.22 µm cellulose acetate filter: i) an aliquot (30 mL) was collected in an acid-cleaned HDPE bottle and acidified with 0.015 M HNO_3 (Suprapur, Merck®) for analysis of Sb concentration and Sb isotope ratio, ii) another aliquot was collected in an acid-cleaned polypropylene tube (10 mL) and stabilized with 20 mM EDTA (J. T. Baker) and 87 mM acetic acid (Suprapur, Merck®) for the analysis of Sb redox speciation. A dilution factor of 10 (CR2, CR3, LUU) or 100 (SJ1, CR1) with ultrapure water was applied for redox speciation of AMD iron-rich waters. This procedure was adapted from Daus and Wennrich (2014) and Wu and Pichler (2016); EDTA, as a complexing agent, sequesters dissolved iron and the acid medium prevents the oxidation of Fe^{2+} in Fe^{3+}. Dilution was performed to remain within the validity limits of the method in terms of iron concentration (<25 $mg.L^{-1}$), to avoid iron precipitation and subsequent Sb adsorption or Sb(III) oxidation (Wu and Pichler, 2016). All stabilized water samples and the 2 L bottle of raw water were stored in the dark in a cool box and brought back for further processing in the UTO (Universidad Tecnica de Oruro). Once in the laboratory, the raw water was filtrated (within 1 hour after sampling) through acid-cleaned, pre-weighed 0.22 µm PVDF filters (Millipore®) fitted on polycarbonate filter holders (Sartorius®) to recover suspended particulate matter (SPM). Filters with SPM were stored in a filter box. Finally, a subsample (20 mL) of the filtrate (< 0.22 µm) was centrifuged in an ultrafiltration unit (< 10 kDa, Vivaspin®, Sartorius®) to obtain the "truly dissolved" phase, and the ultrafiltrated fraction (< 10 kDa) was stored in acid-cleaned HDPE bottle and acidified with 0.015 M of HNO_3 (Suprapur, Merck®) for analysis of Sb concentration. All samples (waters, SPM and sediments) were transported in a cool box and then stored at 4 °C until further processing.

2.3 Chemical analysis

2.3.1 Materials and reagents

Sample preparation for concentration and isotope analyses was carried out in a class 10 000 cleanroom facility. Ultrapure water (Milli-Q®, resistivity > 18.2 MΩ cm, Q-POP Element system, Millipore) was used for all experiments and reagent preparation. All consumables used for Sb analysis and Sb chemical separation (e.g., sample bottles, tubes, SPE cartridge, pipette tips…) were soaked in 10 % v/v analytical grade HNO_3 or HCl, respectively, for 48 h and rinsed three times with ultrapure water before use. 30 % w/w HCl (Suprapur, Merck®), 65–69 % w/w HNO_3 (Analpure, Analityka®) and 40 % w/w HF (Suprapur, Merck®) were used for sample preparation and analysis. Sodium borohydride (1 % w/v), ascorbic acid (analytical grade, Sigma-Aldrich®) and potassium iodide (KI, Suprapur, Merck®) were used for hydride generation. Ethylenediaminetetraacetic acid disodium salt (EDTA) (J. T. Baker) and potassium hydrogen-phthalate (SigmaUltra, 99.95%, Sigma-Aldrich) were used for the mobile

phase in High-Performance Liquid Chromatography. A pure Sb standard solution SPEX (Sb 1000 µg mL^{-1} in 20 % w/w HCl, batch number 24-175SBX) was used as an isotopic standard (Ferrari *et al.*, 2021).

For Sb redox speciation, solutions of Sb(III) and Sb(V) were prepared by dissolving 274.2 mg of potassium antimony(III) oxide tartrate trihydrate (Merck®) and 215.8 mg of potassium hexahydroxoantimonate (Merck®), respectively, in 100 mL of ultrapure water, to obtain a Sb concentration of ~1000 mg L^{-1}. The exact Sb concentrations of these solutions were then determined by Inductively Coupled Plasma Mass Spectrometry (ICP-MS).

2.3.2 Sample preparation

Sediments and filters with suspended particulate matter (SPM) were air-dried in an oven at 40 °C for 48 hours. Sediments were sieved at 2 mm before being powdered in an agate mortar. A subsample (50 mg) was digested using microwave-assisted acid digestion (UltraWAVE, Milestone®) following the protocol detailed for sediments in Ferrari *et al.* (2021). Suspended particulate matter on filters were dissolved in PTFE vials on a hot plate at 100 °C for 24 h with 4 mL of concentrated HNO_3 and 3 mL of concentrated HF. The solution was evaporated to dryness and the residue was re-dissolved in 30 mL of 1.5 M HNO_3. For each set of samples, a procedural blank and a certified reference material of sediment (PACS-3 from the National Research Council NRC, Canada and GSD-3 from the Institute of Geophysical and Geochemical Exploration IGGE, China) were included.

The purification procedure of Sb developed by Ferrari *et al.* (2021) was applied on water (<0.22 µm), digest solutions of SPM and sediments before Sb isotope ratio measurement. This procedure is adapted to a wide range of Sb concentrations and sample matrices including mining water and sediments. Briefly, 100 ng of Sb in a 0.5 M HCl matrix with 10 % w/v KI and ascorbic acid were passed through a thiol-functionalised silica powder cartridge to adsorb Sb. Other metals and trace elements were eluded with 5 mL of 0.5 M HCl and 6 mL of 2.5 M HCl. Finally, Sb was recovered with 6 mL of 6 M HCl. Purification blanks showed that no contamination occurred during the procedure (Sb in blank < 1 ng). After the purification step, Sb recovery was checked by ICP-MS analysis for all 2019 purified samples (Sb recovered at 103 ± 10 %, n=17). The analysis also showed the absence of potentially interfering elements (As, Sn, Te…) that could create analytical bias on Sb isotopic ratio measurement (isobaric and/or polyatomic interferences, matrix effect) (Ferrari *et al.*, 2021). For 2021 samples, Sb recovery (107 ± 11 %, n=20) was calculated based on the intensity measured by HG-MC-ICP-MS compared to the expected Sb intensity (considering dilution factors and an initial Sb mass before purification of 100 ng).

2.3.3 Analytical methods

All the analyses were performed at the laboratory HydroSciences Montpellier and the AETE-ISO platform (OSU OREME, Université de Montpellier).

The concentration of dissolved organic carbon (DOC) was determined using a TOC-VCSH Shimadzu carbon analyser. Total Sb concentration was determined in waters (<10 kDa and < 0.22 µm), sediments and SPM by Inductively Coupled Plasma Mass Spectrometry (ICP-MS, iCAP-TQ, Thermo Scientific®) after an adequate dilution in 0.15 M HNO_3, according to the procedure described in Ferrari *et al.* (2021). Iron and sulphur were also analysed by ICP-MS in these samples because high concentration of these elements is a marker of contamination by AMD. The quality of ICP-MS analysis was checked using certified reference materials (CRM) for total Sb, Fe and S concentrations in water (SLRS-6 from the National Research Council NRC, Canada or NIST 1643e from the National Institute of Standards and Technology, USA) and sediments (PACS-3, GSD-3); concentrations were within 10 % of the certified values. Antimony, Fe and S in digestion blanks were negligible (<1 % of the concentrations in samples). A contamination with 1.7 $\mu g.L^{-1}$ of Sb occurred during the ultrafiltration step but it generally represented less than 10 % of Sb concentration measured in the fraction below 10 kDa of the water samples, except for station PAR (29 %) and LUU (25 %). The blank contribution to Sb concentration in the fraction below 10 kDa was deduced for all samples. The concentration in the colloidal phase (10kDa << 0.22µm) was determined by difference between the concentrations measured in the water samples filtrated at 0.22 µm and ultrafiltrated at 10 kDa.

Determination of Sb(III) and Sb(V) concentrations in the dissolved phase (< 0.22 µm) was carried out by High-Performance Liquid Chromatography coupled to ICP-MS (HPLC-ICP-MS, iCAP-Q, Thermo Scientific®) as described in Resongles *et al.* (2013). The mobile phase consisted of 5 $mmol.L^{-1}$ EDTA and 2 $mmol.L^{-1}$ potassium hydrogen-phthalate, with a pH of around 4.5. Samples were diluted in a 20 mM EDTA and 17 mM acetic acid matrix. An internal standard solution of indium (In, 1 $\mu g.L^{-1}$) was injected continuously after the chromatographic separation and the In signal was used to correct potential sensitivity drifts of ICP-MS. Detection limits were 0.07 $\mu g.L^{-1}$ and 0.04 $\mu g.L^{-1}$ for Sb(III) and Sb(V), respectively. As no CRM is available for Sb redox speciation, the certified water TM-25.5 (from Environment and Climate Change Canada) was measured to check the accuracy of total Sb concentration (sum of the two species Sb(III) and Sb(V)) and was found at 21.1 $\mu g.L^{-1}$ within the range of certified value (20.4-26.6 $\mu g.L^{-1}$).

Antimony isotope ratio was measured in the dissolved phase (< 0.22 µm), SPM and sediments by Hydride Generation Multi-Collector Inductively Coupled Plasma Mass Spectrometry (HG-MC-ICP-MS, Neptune Plus Multi-Collector, Thermo Scientific®). Details of the sample conditioning and analytical settings are presented in Ferrari *et al.* (2021) with minor changes in HG-MC-ICP-MS settings

(suppression of additional gas at the entrance of the HG module, decrease of the argon gas flow to avoid short- and long- term pressure instabilities) to improve signal stability as described in Ferrari et al. (2023). Instrumental settings are presented in Appendix (Table S2). Briefly, samples were diluted to 2 µg.L^{-1} of Sb in 3 M HCl with 0.5 % w/v of KI-ascorbic acid, at least 3 hours before the analysis. Each sample was analysed 3-times using the sample-standard bracketing method with the SPEX isotopic standard solution. ^{121}Sb and ^{123}Sb were measured together with ^{120}Sn, ^{122}Sn and ^{126}Te to check that no interference occurred. A correction of ^{123}Te (isotope abundance of 0.91 %) interference on ^{123}Sb was not required as ^{126}Te (isotope abundance of 19.0 %) intensity was 0.06 mV on average (<0.01 % of ^{123}Sb intensity). Blank solution (3 M HCl with 0.5 % w/v of KI-ascorbic acid) represented less than 1 % of Sb signal intensity of standard solution and samples.

Antimony isotopic composition is expressed as δ^{123}Sb notation (Equation 1) and is the average value for the three isotopic measurements if not specified otherwise.

$$\delta^{123}Sb(‰) = \left(\frac{\left(\frac{^{123}Sb}{^{121}Sb}\right)_{sample} - \left(\frac{^{123}Sb}{^{121}Sb}\right)_{mean\ std}}{\left(\frac{^{123}Sb}{^{121}Sb}\right)_{mean\ std}}\right) \times 1000 \quad \text{(Eq. 1)}$$

Where $\left(\frac{^{123}Sb}{^{121}Sb}\right)_{mean\ std}$ is the average of the Sb isotope ratio of the Sb isotope standard solution SPEX measured before and after the sample.

The quality of Sb isotope measurement was checked by measuring the Sb isotopic composition of certified reference material published in Ferrari et al. (2021). Two certified reference materials (CRM) of sediments, PACS-3 (National Research Council NRC, Canada) and GSD-3 (Institute of Geophysical and Geochemical Exploration IGGE, China), were measured at 0.14 ± 0.06 ‰ and 0.15 ± 0.04 ‰, respectively, matching the previously published values (Ferrari *et al.,* 2021).

3. Results

3.1 Main physicochemical parameters, Sb concentration and speciation

3.1.1 Geochemical background

Reference samples from Paria (PAR) and Cala-Cala (CC) rivers (representative of the geochemical background, sampled during the 2021 dry season) exhibited near-neutral pH of 8.30 and 7.29, respectively (Table 1). Conductivity in Cala-Cala River was 422 µS.cm^{-1} and was relatively high in Paria River (1125 µS.cm^{-1}), although lower than at contaminated sites. Redox potential (336 mV) revealed oxidizing conditions at both reference stations; a low dissolved oxygen (DO) value (1.7 mg.L^{-1}) was measured in Cala-Cala River, which could be attributed to groundwater contribution to surface

waters at the end of the dry season. The concentrations of DOC (≤ 6.6 mg.L^{-1}), dissolved Sb (≤ 4.1 µg.L^{-1}), dissolved Fe (≤ 0.5 mg.L^{-1}) and dissolved S (≤ 48 mg.L^{-1}) were lower than those measured at contaminated sites (Figure 2a). At the station PAR, Sb was present in a true dissolved form in water (i.e., same concentration in the fraction filtered at 0.22 µm and ultrafiltered at 10 kDa, Table 1). The concentration of Sb in the solid phase was 20.9 mg.kg^{-1} (PAR) in suspended particulate matter (SPM) and from 16.3 mg.kg^{-1} (CC) to 20.4 mg.kg^{-1} (PAR) in sediments, close to the background value of 12 ± 2 mg.kg^{-1} determined in the same area by Tapia et al. (2012).

Table 1: Main physico-chemical parameters, concentrations of Sb (total Sb and proportion of Sb(III) and Sb(V) in water < 0.22 µm), Fe, S, DOC, and Sb isotope ratio (δ^{123}Sb ±- 2σ) in water (< 0.22 µm), SPM and sediments from the rivers at the end of the wet (March 2019) and dry (October 2021) seasons.

	San José mine AMD				Canal Rosso				Lake Uru-Uru		Vinto River				Urban Canal	Paria River	Cala-Cala River
	SJ1		CR1		CR2		CR3		LUU		V1		V2		URB	PAR	CC
Season:																	
WS Wet Season (2019)	**WS**	**DS**	**WS**	**DS**	**WS**	**DS**	**WS**	**DS**	**WS**	**DS**	**WS**	**DS**	**WS**	**DS**	**DS**	**DS**	**DS**
DS Dry Season (2021)																	
Water physico-chemical parameters																	
Temperature (°C)	-	22.8	-	15.3	-	11.8	-	9.4	-	25.5	-	-	-	-	14.5	11.5	15.2
pH	1-2	1.56	2	1.85	4-5	4.48	5	5.23	7	6.51	6-7	-	7	-	7.90	8.30	7.29
Eh (mV)[a]	-	616.8	-	602.5	-	412.5	-	350.4	-	175.5	-	-	-	-	2.3	336.7	336.3
Conductivity ($\mu S.cm^{-1}$)	-	93300	-	65700	-	13450	-	14710	-	18300	-	-	-	-	5410	1125	422
DO ($mg.L^{-1}$)	-	4.54	-	5.21	-	4.64	-	2.46	-	2.75	-	-	-	-	0.14	7.07	1.71
River water (< 0.22 µm)																	
DOC ($mg.L^{-1}$)	-	12.0	-	44.5	-	65.9	-	55.2	-	45.2	-	-	-	-	21.9	6.6	3.5
Fe ($mg.L^{-1}$)	3114	3716	1768	2930	291	249	164	233	0.18	122	0.03	-	0.06	-	4.47	0.50	0.005
S ($mg.L^{-1}$)	3651	4258	2673	3965	962	499	691	549	522	679	35	-	40.8	-	251	48.1	34.1
Sb ($\mu g.L^{-1}$)	7824	8057	2242	4070	24.8	97.4	10.2	19.9	21.9	7.2	31.4	-	33.3	-	18.5	4.12	2.01
Sb(III) (%)	-	19.4	-	9.5	-	<0.9[b]	-	<4.8[b]	-	<13.1[b]	-	-	-	-	15.8	<2.6[b]	<5.2[b]
Sb(V) (%)	-	80.6	-	90.5	-	>99.1	-	>95.2	-	>86.9	-	-	-	-	84.2	>94.4	>94.8
$\delta^{123}Sb$ (‰)	0.46 ± 0.02	0.42 ± 0.02	0.42 ± 0.07	0.43 ± 0.01	0.55 ± 0.04	0.54 ± 0.02	0.60 ± 0.02	0.70 ± 0.03	0.28 ± 0.02	0.55 ± 0.01	0.29 ± 0.02	-	0.36 ± 0.03	-	0.61 ± 0.06	0.36 ± 0.04	0.33 ± 0.02
Suspended particulate matter (> 0.22 µm)																	
SPM concentration ($mg.L^{-1}$)	-	38.4	-	*(369)*[c]	-	47.3	-	51.9	-	7061	-	-	-	-	63.9	14.6	-
Fe ($mg.kg^{-1}$ d.w.)	-	51139	-	74432	-	60562	-	217148	-	88149	-	-	-	-	14458	39524	-
S ($mg.kg^{-1}$ d.w.)	-	<270000[d]	-	<72000[d]	-	<34400[d]	-	<19700[d]	-	<11200[d]	-	-	-	-	75080	<14000[d]	-
Sb ($mg.kg^{-1}$ d.w)	-	2614	-	3837	-	262	-	94.3	-	24.1	-	-	-	-	28.6	20.9	-
$\delta^{123}Sb$ (‰)	-	0.26 ± 0.02	-	0.32 ± 0.02	-	0.31 ± 0.01	-	0.49 ± 0.05	-	0.31 ± 0.04	-	-	-	-	-	-	-
Sediments (< 2 mm)																	
Fe ($mg.kg^{-1}$)	166029	14083	44242	80463	64852	38535	45924	94766	71221	82061	36993	28140	31923	36032	52446	24567	25394
S ($mg.kg^{-1}$)	201750	<550000[d]	51601	<96000[d]	10547	<12000[d]	35418	25314	13317	<6100[d]	<686[d]	<2500[d]	<626[d]	<21000[d]	17412	<1100[d]	<1100[d]
Sb ($mg.kg^{-1}$)	14528	715	211	1431	203	273	57.2	259	82.1	47.3	154	34.9	419	78.2	54.7	20.4	16.3
$\delta^{123}Sb$ (‰)	-0.09 ± 0.02	0.22 ± 0.02	0.08 (n=1)	0.36 ± 0.02	0.23 ± 0.05	0.23 ± 0.03	0.23 ± 0.04	0.25 ± 0.02	0.22 ± 0.05	0.20 ± 0.04	0.03 ± 0.08	0.18 ± 0.05	0.23 ± 0.03	0.13 ± 0.06	0.11 ± 0.04	0.13 ± 0.05	0.24 ± 0.07

[a]Measured redox potential was corrected to give redox potentials relative to a Normal Hydrogen Electrode (NHE).

[b]Sb(III) was below detection limit (<detection limit (0.07 $\mu g.L^{-1}$) x dilution factor for IC-ICP-MS analysis)

[c]The proportion of Sb associated with the particulate fraction at the CR1 station represents an overestimate because bottom sediments were resuspended during the sampling due to the low water column and the inaccessibility of the site (covered canal accessible only through a manhole cover)

[d]Sulphur concentration (< detection limit (150 $\mu g.L^{-1}$) x dilution factor for ICP-MS analysis).

Figure 2: a) Spatial variation of Sb concentration and Sb isotopic composition in water (<0.22 µm) and b) spatial variation of Sb concentration and Sb isotopic composition in sediments.

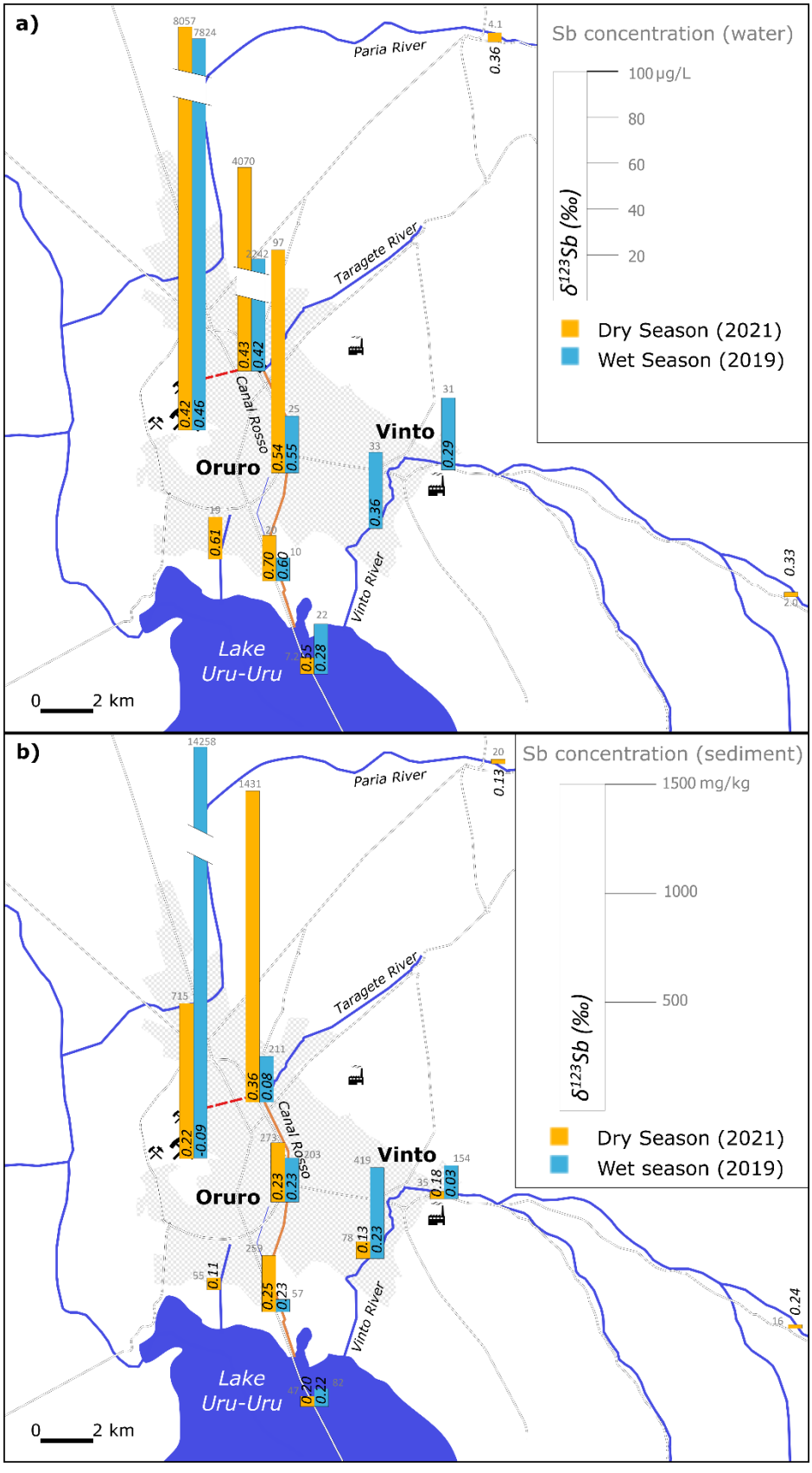

3.1.2 AMD-Lake continuum

Station SJ1 consisted of a shallow yellowish AMD at the outlet of San Jose mine gallery, with a low pH (1.56), a very high conductivity (93.3 $mS.cm^{-1}$), high concentrations of dissolved Fe and S, up to 3.7 $g.L^{-1}$ and 4.3 $g.L^{-1}$ during the dry season, respectively (Table 1). Redox and DO values (Eh = 616.8 mV and DO = 4.54 $mg.L^{-1}$) reflected oxidizing conditions. Dissolved antimony concentrations were 7.8 $mg.L^{-1}$ (wet season) and 8 $mg.L^{-1}$ (dry season). During the dry season, Sb was mainly in the oxidized form (80.6 % Sb(V) and 19.4 % Sb(III)) and mainly present as truly dissolved Sb (98 %) in the water column (Table 1). Antimony concentration in the sediments at SJ1 was extremely high during the wet season (14259 $\mu g.kg^{-1}$) and was associated with a high Fe (16.6 wt.%) and S (20.2 wt.%) content. Antimony, Fe and S concentrations were lower (715 $\mu g.kg^{-1}$, 1.4 wt.% and 4.4 wt.%, respectively) during the dry season (Figure 2b). The two samples from the San José mining waste heaps were also heterogeneous in terms of Sb concentration (128 $mg.kg^{-1}$ and 2604 $mg.kg^{-1}$), Fe concentration (4.2 wt.% to 11.3 wt.%), and S concentration (1.7 wt.% and 10.9 wt.%) (Table S3).

From station SJ1 to downstream stations CR1, CR2 and CR3 in Canal Rosso, important physico-chemical changes occurred. The pH continuously increased up to 5.2, while conductivity decreased down to 14.7 $mS.cm^{-1}$ (Table 1). Dissolved Fe and S concentrations dropped by one order of magnitude. Redox and DO values decreased down to 350 mV and 2.5 $mg.L^{-1}$ (CR3), respectively, while DOC concentration increased from 12 $mg.L^{-1}$ (SJ1) to 66 $mg.L^{-1}$ (CR2) in relation to untreated domestic wastewater inputs. Dissolved Sb concentrations decreased by at least two orders of magnitude compared to SJ1, down to ≤ 20 $\mu g.L^{-1}$ at CR3 station (Figure 2a). In water, Sb was in a truly dissolved form (no significant difference between the concentration of Sb in the dissolved phases <0.22 µm and < 10 kDa, Table 1). Antimony(V) was predominant (≥ 90.1 %) ; Sb(III) was no more detected downstream from station CR1 (Table 1). Antimony exhibited high concentration in SPM (up to 3837 $\mu g.kg^{-1}$ at CR1) and sediments (from 57 to 1431 $\mu g.kg^{-1}$) at stations CR1, CR2 and CR3, in association with a high Fe content (6.1 to 21.7 wt.% in SPM, 3.9 to 9.5 wt.% in sediment) and S content (1.1 to 5.2 wt.% in sediment) (Table 1). In the water column, Sb was mainly in the truly dissolved phase (Table 1, Figure 3). Particulate Sb represented up to 20 % of total Sb concentration in the raw water, while the colloidal Sb phase (between 10 kDa and 0.22 µm) was negligible (≤ 1 % of total Sb) (Figure 3).

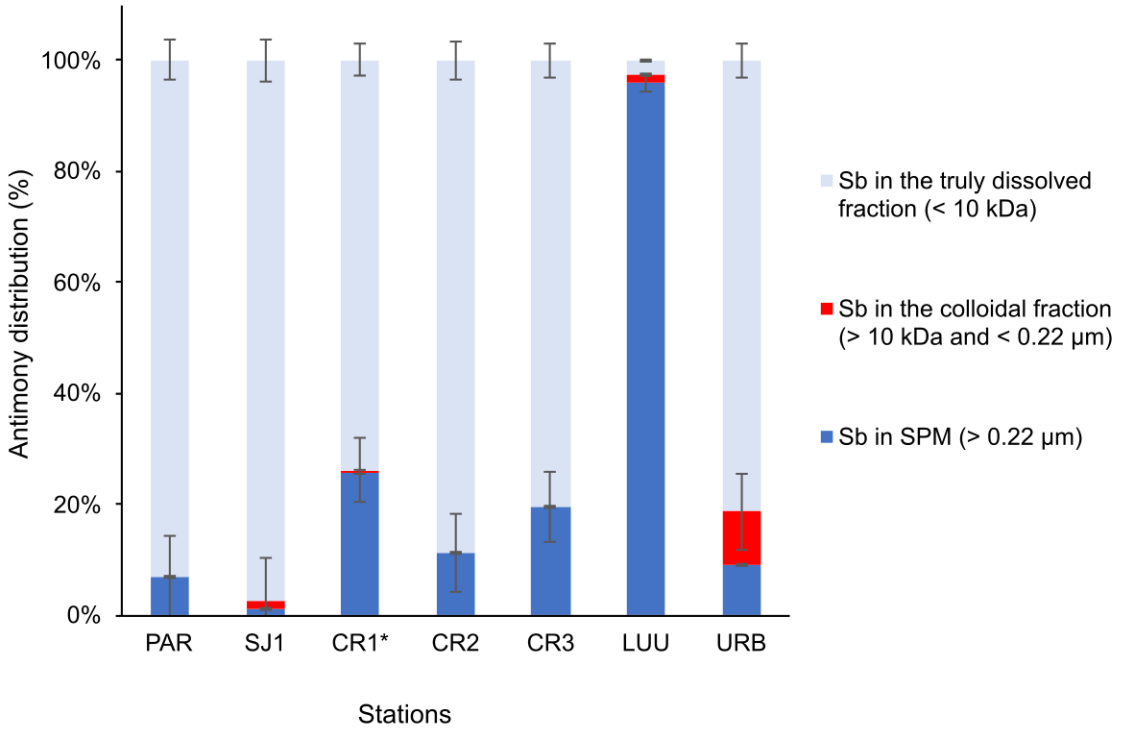

*Figure 3: Distribution of Sb (in %) in the water column among the truly dissolved (<10 kDa), colloidal (> 10 kDa and < 0.22 µm) and particulate (> 0.22 µm) phases. The colloidal phase was calculated by the difference between Sb concentrations in the dissolved phase filtrated at 0.22 µm and ultrafiltrated at 10 kDa. *The proportion of Sb associated with the particulate phase at the CR1 station represents an overestimate because bottom sediments were resuspended during the sampling due to the low water column and the inaccessibility of the site (covered canal accessible only through a manhole cover). Uncertainties (error bars) were estimated by propagating the analytical uncertainty of ICP-MS measurement to the distribution calculation (relative standard deviation (RSD) of 4 % and 1.5 % were applied to water samples (<0.22 µm and < 10 kDa) and SPM samples, respectively, based on the RSD measured for the certified reference materials of water (SLRS-6) and sediment (PACS-3) analysed alongside the samples.*

3.1.3 Lake Uru-Uru

The Lake Uru-Uru (LUU) exhibited a higher pH (6.51) and lower dissolved Fe concentration than Canal Rosso, that flows into it. Redox (Eh = 175.5 mV) and DO value (2.75 $mg.L^{-1}$) showed weakly oxidising conditions, in relation with a high DOC concentration (45.2 $mg.L^{-1}$). Dissolved Sb concentration showed a decrease from the most downstream station in Canal Rosso CR3 (19.9 $\mu g.L^{-1}$) to the lake LUU (7.2 $\mu g.L^{-1}$ of which 4.7 µg/L in a truly dissolved form) in the dry season, while it showed an increase (from 10.2 to 21.9 $\mu g.L^{-1}$) in the wet season. Antimony(V) predominated in the lake. The same trend was observed for Sb concentration in sediments, with either a decrease from CR3 (259 $mg.kg^{-1}$) to LUU (47.3 $mg.kg^{-1}$) in the dry season or an increase (from 57.2 to 82.1 $mg.kg^{-1}$) in the wet season (Table 1, Figure 2b). The concentration of SPM was extremely high, around 7 $g.L^{-1}$; SPM contained 24.1 $mg.kg^{-1}$ of Sb, in association with 8.8 wt.% Fe, thus particulate Sb represented 96 ± 3 % of total Sb in the raw lake water. The colloidal phase was negligible (≤ 1 % of total Sb) in the water column although it represented 35 % of Sb in filtrated water (2.5 µg/L) (Figure 3).

3.1.4 Urban Canal

The Urban Canal (URB), which collected domestic wastewaters, exhibited a circumneutral pH (7.90) and high conductivity (5.4 $mS.cm^{-1}$). Low redox (Eh = 2.3 mV) and DO (0.14 $mg.L^{-1}$) values reflected reducing conditions, in relation with the high DOC value (22 $mg.L^{-1}$). Dissolved Fe and S concentrations of 4.47 $mg.L^{-1}$ and 251 $mg.L^{-1}$ respectively, were lower than in Canal Rosso but higher than in reference stations PAR and CC, which likely reflect AMD contamination. Dissolved Sb concentration of 18.5 $\mu g.L^{-1}$ was similar to the most downstream station in Canal Rosso (CR3), but redox speciation differed, showing 16 % Sb(III). Particulate and sedimentary Sb concentrations of 28.6 $mg.kg^{-1}$ and 54.7 $mg.kg^{-1}$ respectively were at least three times lower than in CR3. The colloidal phase represented ~10 % of total Sb (2 µg/L), which contrasted with the lack of colloidal Sb in Canal Rosso and lake Uru-Uru and probably reflected organic-mineral association in this sewage effluent (Figure 3).

3.1.5 Vinto River

The intermittent Vinto river that flowed next to the smelter site (station V1) and further downstream (V2) exhibited near-neutral pH (6-7) and low concentrations of dissolved Fe (≤ 0.06 $mg.L^{-1}$) and dissolved S (≤ 41 $mg.L^{-1}$), similarly to reference stations PAR and CC ([Fe] ≤ 0.5 $mg.L^{-1}$, [S] ≤ 48 $mg.L^{-1}$). Dissolved Sb concentrations were higher at stations V1 (31.4 $\mu g.L^{-1}$) and V2 (33.3 $\mu g.L^{-1}$), than at the upstream reference station CC (2.01 $\mu g.L^{-1}$), showing an influence of the smelter area. The sediments at stations V1 and V2 also showed a higher Sb content (35 and 78 $mg.kg^{-1}$ during the dry season and 154 and 419 $mg.kg^{-1}$ during the wet season) than at the reference station CC (16.3 $mg.kg^{-1}$). The composite sample representative of smelter slags had a relatively low Sb content (41.7 $mg.kg^{-1}$ Sb) compared to mining wastes and a higher Fe content (21 wt. % Fe). Direct input of liquid effluent from the smelter was not observed; an input of contaminated groundwater and leaching of soils contaminated by atmospheric fallout could be involved instead.

3.1.6 Drinking water

Samples from the Vinto drinking water network (DW1-3) exhibited Sb concentrations between 7 and 8.3 $\mu g.L^{-1}$ (Table 2), thus slightly above the geochemical background determined for surface waters (≤ 4 $\mu g.L^{-1}$ at stations PAR and CC). Sample from the Oruro drinking water network (DW0) presented a lower Sb concentration (0.42 $\mu g.L^{-1}$). The low concentrations of dissolved Fe (0.5 – 0.6 $mg.L^{-1}$) and dissolved S (0.05 – 0.1 $mg.L^{-1}$) at all DW stations denoted the lack of AMD contamination.

Sample name	DW0	DW1	DW2	DW3
Fe ($mg.L^{-1}$)	0.52	0.49	0.64	0.50
S ($mg.L^{-1}$)	0.05	0.10	0.11	0.13
Sb ($\mu g.L^{-1}$)	0.42	7.99	8.35	7.04
$\delta^{123}Sb$ (‰)	n.d.	0.64 ± 0.03	0.67 ± 0.02	0.93 ± 0.01

Table 2: Drinking water in the city of Oruro (DWO) and Vinto (DW1, DW2 and DW3).

3.2 Antimony isotopic composition

Antimony isotopic composition ($\delta^{123}Sb$) in the various samples (water, SPM, sediments, mine wastes and smelter slags) collected in the study area ranged from -0.09 to +0.93 ‰. The mine waste samples exhibited an Sb isotopic composition ($\delta^{123}Sb$) of 0.14 ± 0.07 ‰ and 0.17 ± 0.08 ‰, while the Vinto smelting slag was slightly isotopically higher, with a signature of 0.29 ± 0.04 ‰. Water sampled at the reference sites Cala-Cala and Paria, representative of the geochemical background, exhibited similar isotopic composition ($\delta^{123}Sb$ = 0.33 ± 0.02 ‰ and 0.36 ± 0.04, respectively), significantly different from the Canal Rosso values ($\delta^{123}Sb$ = 0.4 – 0.7 ‰), but similar to the Vinto River value ($\delta^{123}Sb$ ≈ 0.3 ‰). The sediments at PAR and CC stations exhibited lower $\delta^{123}Sb$ values than dissolved Sb (0.13 ± 0.05 ‰ and 0.24 ± 0.07 ‰, respectively).

Antimony isotopic composition in water (< 0.22 µm) increased from the San José mine ($\delta^{123}Sb$ = 0.42 to 0.46 ‰ at SJ1) to downstream stations ($\delta^{123}Sb$ = 0.60 to 0.70 ‰ at CR3) along the river continuum and then decreased ($\delta^{123}Sb$ = 0.28 to 0.55 ‰) in lake Uru-Uru (Figure 2a, Figure S1). The same spatial trend was observed during the wet and dry seasons, although the decrease in Lake Uru-Uru was more significant in the wet season ($\delta^{123}Sb$ = 0.28 ‰) than in the dry season ($\delta^{123}Sb$ = 0.55 ‰). Sediments at the mine gallery exit (SJ1) and the CR1 station exhibited a different Sb isotope signature in the wet and dry seasons ($\Delta^{123}Sb_{dry\text{-}wet}$ ≈ 0.3 ‰), with the lowest isotope signature in the wet season ($\delta^{123}Sb$ = -0.09 ‰ at SJ1 and 0.08 ‰ at CR1) compared to the dry season ($\delta^{123}Sb$ = 0.22 ‰ at SJ1 and 0.36 ‰ at CR1) (Figure 2b). At downstream stations along Canal Rosso and Lake Uru-Uru (CR2, CR3, LUU), Sb isotopic composition in sediments remained relatively stable at 0.23 ± 0.02 ‰, both in the wet and dry seasons. At these stations, SPM showed a slightly higher Sb isotopic composition (0.31 to 0.49 ‰) than the sediments. The surface waters along the river continuum between the mine gallery exit (SJ1), the Canal Rosso (CR1, CR2, CR3) and Lake Uru-Uru (LUU) were preferentially enriched in heavier Sb isotope compared to SPM or sediments (Table 1, Figure S1). On average, the apparent fractionation factor between sediment or SPM and dissolved Sb (< 0.22 µm) was $\Delta^{123}Sb_{water\text{-}sediment}$ = 0.30 ± 0.15 ‰ and $\Delta^{123}Sb_{water\text{-}SPM}$ = 0.21 ± 0.04 ‰, respectively (excluding CR1 from SPM samples due to sediment resuspension during sampling).

Water in the urban canal (URB) exhibited $\delta^{123}Sb$ values of 0.61 ± 0.06 ‰, close to the Canal Rosso values while the sediments had a lower $\delta^{123}Sb$ value (0.11 ± 0.04 ‰) than those of Canal Rosso. Water in the Vinto River downstream from the Vinto smelter exhibited an Sb isotopic composition of around 0.3 ‰, thus significantly lower than the Canal Rosso values but similar $\delta^{123}Sb$ values in sediments (0.08 to 0.23 ‰).

Samples from the Vinto drinking water network exhibited variable Sb isotopic composition from 0.64 ‰ to 0.93 ‰ (Table 2), thus significantly higher than the surface water geochemical background ($\delta^{123}Sb \approx 0.35$ ‰); two samples exhibited a $\delta^{123}Sb$ value similar to that of Canal Rosso ($\delta^{123}Sb = 0.64 \pm 0.03$ ‰ for DW1 and 0.67 ± 0.02 ‰ for DW2), while the third DW sample stood out from all the others, with the highest value of all the data set ($\delta^{123}Sb = 0.93 \pm 0.01$ ‰ for DW3).

4. Discussion

4.1 Variations of Sb isotopic composition in relation with geochemical processes

Antimony concentrations at the exit of the San José mine gallery and in Canal Rosso were among the highest measured in AMD environments worldwide (Filella *et al.*, 2001; Li *et al.*, 2020; Long *et al.*, 2022). The values were roughly the same between the dry and wet seasons and similar to those measured in 2011 by Goix (2012), showing persistent and steady AMD contamination. The decrease of dissolved Sb concentration and concomitant increase of particulate and sedimentary Sb along Canal Rosso reflected natural attenuation of the dissolved Sb contamination. This process involves Sb sorption or coprecipitation with Fe upon pH neutralisation, it was described in other Sb-rich AMD (Manaka *et al.*, 2007; Filella *et al.*, 2009; Resongles *et al.*, 2013). Redox speciation showed that the decrease of dissolved Sb concentration in the AMD was accompanied by a decrease in the percentage of dissolved Sb(III), which reflected Sb(III) oxidation and/or preferential sorption/precipitation of Sb(III) upon Sb(V). Greater retention of Sb(III) during AMD neutralisation was observed in other AMD (Resongles *et al.*, 2013). The natural attenuation process, besides dilution, resulted in relatively low Sb concentration values in both dissolved and particulate/sedimentary phases in lake Uru-Uru, only twice (for dissolved phase and sediment) those measured at the reference sites representative of the geochemical background.

The isotopic composition of antimony in the AMD water of the San José mine, at the gallery exit (SJ1), was heavier than that of two Sb-rich mine wastes and sediments at the same station (Table S3), suggesting that the oxidative dissolution of sulphide minerals preferentially releases the heavy Sb isotope in water. Tanimizu *et al.*, (2011) measured an apparent fractionation factor between water and stibnite $\Delta^{123}Sb_{aqueous\text{-}mineral}$ of +0.35 ‰. The $\Delta^{123}Sb_{aqueous\text{-}mine\ waste}$ at the station SJ1 was between 0.25

and 0.32 ‰, which is consistent with the previous observation of Tanimizu *et al.*, (2011). Recent leaching experiments have confirmed that weathering of stibnite produces a leachate enriched with the heavy Sb isotope by up to 0.5 ‰ (Kaufmann et al., 2024). The origin of Sb isotopic fractionation was ascribed to the precipitation of isotopically light secondary Sb minerals rather than to the dissolution process of stibnite itself which did not fractionate Sb isotopes (Kaufmann et al., 2024). Important differences in the isotopic composition of the sediments in SJ1 were noted between the dry and the wet season $\Delta^{123}Sb_{dry\text{-}wet}$ = +0.31 ‰. This difference is associated with higher Sb concentrations during the wet season (14528 mg.kg^{-1}) than during the dry season (715 mg.kg^{-1}) and is likely explained by a difference in the nature of the sampled sediments. Indeed, a large range of isotopic composition have been found in secondary Sb minerals (from -0.50 ‰ to +0.69 ‰) resulting from stibnite dissolution (Kaufmann et al., 2024). Based on visual observations and sulphur content (representing 20 % of dry weight), grey sediments sampled in the AMD stream at the exit of the San José mine in the wet season likely consisted of primary minerals (sulphides) exploited in the mine while yellow sediments sampled in the dry seasons were likely dominated by secondary neoformed minerals. Goix et al. (2012) highlighted the presence of exploited sulphides in the AMD at the San José mine exit (including Sb sulphides such as boulangerite and andorite) in addition to secondary Fe and Al sulphates and Fe (oxyhydr)oxides (ferrihydrite, goethite, hematite) minerals while primary sulphides were no longer detected further downstream.

The apparent fractionation factor between water and sediment in Canal Rosso $\Delta^{123}Sb_{water\text{-}sediments}$ was 0.28 ± 0.19 ‰ in the dry season and 0.34 ± 0.03 ‰ in the wet season, considering the three stations (CR1, CR2, CR3). In acid mine drainage, one of the most important factors controlling the mobility of Sb is its sorption onto Fe-, Al-, or Mn- oxyhydroxides due to the important specific surface area of these phases (Fukushi *et al.*, 2003; Manaka *et al.*, 2007). These processes play an important role in the immobilisation of Sb in the sediments (Hiller *et al.*, 2012). Recently, Sb(V) (Zhou *et al.*, 2023; Ferrari et al., 2024) and Sb(III) (Ferrari et al., 2024) equilibrium isotopic fractionation was experimentally studied during their adsorption on Fe minerals including ferrihydrite ($\Delta^{123}Sb_{aqueous\text{-}adsorbed}$= 0.25-0.49 ‰), schwertmannite (($\Delta^{123}Sb_{aqueous\text{-}adsorbed}$=0.27-0.36 ‰), goethite ($\Delta^{123}Sb_{aqueous\text{-}adsorbed}$= 1.14 ‰) and hematite ($\Delta^{123}Sb_{aqueous\text{-}\ adsorbed}$= 1.12 ‰). The apparent fractionation factors ($\Delta^{123}Sb_{water\text{-}sediments}$) determined between the dissolved and sedimentary antimony in the AMD along Canal Rosso in the present study matched the equilibrium isotopic fractionation factors measured for Sb(III) and Sb(V) adsorption on these first two iron oxyhydroxide and oxyhydroxysulphate phases typical of AMD-impacted streams at acidic (schwertmannite) and near-neutral (ferrihydrite) pH (Bigham *et al.*, 1996), although they are lower than the fractionation value reported by Zhou *et al.* (2023) for ferrihydrite. The progressive increase of $\delta^{123}Sb$ in water and SPM or sediments along the

AMD stream (stations SJ1 to CR3), concomitant with a decrease of dissolved Sb concentration (Figure S1), was thus likely related to the adsorption of Sb on (oxy)hydroxides. The progressive depletion of light isotopes in the dissolved phase resulted in a progressive increase of $\delta^{123}Sb$ of newly sorbed Sb in SPM and sediments (Figure S1). These results contrast with the steady isotope signature observed in the river water of mine-affected streams in France and China which was explained in both cases by the conservative behaviour of Sb in these near-neutral rivers (Resongles et al., 2015; Wen et al., 2023, Liu et al., 2024).

The urban canal (URB) showed lower Sb concentrations in water, SPM and sediments than the Canal Rosso that directly received AMD from the San José mine gallery; however, they were significantly higher than the geochemical background; furthermore, the high Fe concentrations in water, SPM and sediment were characteristic of AMD chemistry, which confirmed AMD input. The apparent fractionation factor between dissolved and sedimentary Sb ($\Delta^{123}Sb_{water\text{-}sediments}$ of +0.50 ‰) was higher than in Canal Rosso. The mixing of AMD with wastewater effluent in the urban canal may involve other (organic-rich) solids with a different adsorption isotopic fractionation factor as the extent of Sb fractionation is known to vary with the nature of the mineral phase and the adsorption mechanism involved (Zhou *et al.*, 2022, 2023, 2024). Alternatively, other (bio-)geochemical processes, besides sorption on Fe secondary minerals, could be involved in Sb isotopic fractionation in these reducing waters. Indeed, a recent experimental study observed a Sb isotope fractionation of the same extent (fractionation factor of -0.46 to -0.62 ‰) due to Sb(V) reduction by sulphides and subsequent Sb(III) sulphide precipitation under conditions relevant to the station URB (i.e., circumneutral pH of 5-8, sulphur concentration 32-192 $mg.L^{-1}$) (Veldhuizen *et al.,* 2023).

The smelting slag sample exhibited a $\delta^{123}Sb$ value of 0.29 ± 0.04 ‰, similar to the geochemical background represented by Cala-Cala river sediment (0.24 ± 0.07 ‰). High-temperature processes usually fractionate metal isotopes (e.g. Cd, Zn), with enrichment in the light isotopes in the atmospheric dust and enrichment in the heavy isotopes in slags (Sonke *et al.*, 2008; Wiederhold, 2015). For Sb isotopes, the fractionation associated with smelting is not well characterized and understood yet. However, two recent studies revealed contradictory results probably due to differences in the smelting process. Indeed, a first study measuring Sb isotopes in slag, dust and ore from a modern industrial Sb smelter did not observe significant Sb isotopic fractionation due to smelting (Liao *et al.*, 2023), similarly to the present study, while a second study carried out at an old (>100 yrs.) small-scale Pb smelting site revealed a large fractionation between slags and ore (Guillevic et al., 2024). A better characterisation of the processed ore and fume dust would be required to better understand Sb isotope fractionation associated with high temperature industrial processes.

560 **4.2 Variations of Sb isotopic composition associated with different contamination sources**

561 The contrasting isotopic signature of dissolved antimony in DMA water from the Canal Rosso
562 at the most downstream station (CR3, $\delta^{123}Sb$ = 0.60 - 0.70 ‰) and in river water downstream from the
563 Vinto smelter (V2, $\delta^{123}Sb$ = 0.36 ‰) could potentially provide information on the contribution of these
564 two different anthropogenic sources to the Lake Uru-Uru. Water from the lake Uru-Uru exhibited a
565 significant change in Sb isotopic composition between the wet and dry periods. During the dry period
566 (2021), the signature (0.55 ± 0.01 ‰) was close to that of the AMD (> 0.4 ‰). During the wet period
567 (2019), the signature (0.28 ± 0.02 ‰) was closer to that of the Vinto River water (0.29-0.36 ‰). Thus,
568 the isotopic contribution of these two different sources (the AMD-impacted river and the smelting-
569 impacted river) might produce the isotopic composition in the Uru-Uru Lake water. This hypothesis of
570 an additional 'smelting-affected river' source during the wet season is also supported by the increase
571 of Sb concentration from 10 $\mu g.L^{-1}$ in the Canal Rosso (at CR3) to 21.7 $\mu g.L^{-1}$ in the lake (LUU) observed
572 during the wet season when the smelting-affected river flowed while the concentration between these
573 two stations decreased during the dry season when the Vinto river was not flowing. The Sb isotopic
574 composition of LUU sediments did not vary with the season, with $\delta^{123}Sb$ around 0.2 ‰, which was
575 close to Canal Rosso sediments ($\delta^{123}Sb$ = 0.2 – 0.3 ‰) and Vinto river sediments ($\delta^{123}Sb$ = 0.1 – 0.2 ‰).
576 In the urban canal, dissolved Sb concentration of 18.5 $\mu g.L^{-1}$ was higher than the geochemical
577 background (≤ 4 $\mu g.L^{-1}$) and $\delta^{123}Sb$ of ~0.6 ‰ was close to that of Canal Rosso ($\delta^{123}Sb$ = 0.4-0.7 ‰),
578 which suggests that Sb enrichment in this canal originates from AMD input.

579 The Sb concentration of the drinking water samples in the Vinto area (7 – 8 $\mu g.L^{-1}$) was higher
580 than that of the local geochemical background for surface waters represented by the Cala-Cala and
581 Paria rivers (2 – 4 $\mu g.L^{-1}$), which likely denoted anthropogenic contamination. However, the Sb isotopic
582 composition, $\delta^{123}Sb$ = 0.6 – 0.9 ‰, differs from that of the Vinto river downstream the smelter ($\delta^{123}Sb$
583 = 0.3 – 0.4 ‰), suggesting another contamination source or fractionation of Sb isotopes during
584 groundwater – surface water interactions. According to the local people, the drinking water in Vinto is
585 from groundwater pumped in Cala-Cala and Sepulturas, close to the smelter localities. It is delivered
586 with no treatment (other than disinfection). Therefore, contamination of drinking water by smelter
587 discharges could be expected. The contrasted $\delta^{123}Sb$ value between drinking water originating from
588 local groundwater and Vinto river water suggested that natural processes occur between surface
589 water and groundwater or within the aquifer (redox change, adsorption) that modify $\delta^{123}Sb$ value. Such
590 a difference between the isotopic composition of industrial effluents contaminating an aquifer and the
591 isotopic composition of groundwater has been observed for Cr and was mainly explained by isotope
592 fractionation due to Cr(VI) reduction within the aquifer (Novak et al. 2017; Slejko, et al. 2019). Further
593 research is needed to understand the origin of such an Sb isotope shift.

5. Conclusion

This field study is among the first to document Sb isotope composition variability in a mining and industrial multi-source context. It documented a range of Sb isotope composition between -0.09 and +0.93 ‰, with significant difference between dissolved Sb in AMD (0.4 – 0.7 ‰) and dissolved Sb in a smelter-impacted stream (~0.3 ‰). It showed that natural attenuation process in AMD produced significant Sb isotope fractionation between Sb in the dissolved phase and the solid ($\Delta^{123}Sb_{water\text{-}sediments}$ ~ 0.3 ‰) that reflected sorption of Sb(III) and Sb(V) on secondary Fe-oxyhydroxides, privileging the light Sb isotope. The study also showed significant variation of Sb isotope composition between dry period ($\delta^{123}Sb$ = 0.55 ± 0.01 ‰) and wet period ($\delta^{123}Sb$ = 0.28 ± 0.02 ‰) in Uru-Uru lake water, which most readily reflected a variable contribution from the different tributaries impacted by distinct Sb sources, namely the AMD-impacted river of Oruro and the smelter-impacted river of Vinto.

Altogether, these results show that Sb isotopes have the potential to help tracking Sb sources and transport processes in mining areas. An in-depth characterisation of Sb geochemistry (concentration, speciation and distribution), as done in this study, in complement to the determination of Sb isotope composition, is essential to achieve a comprehensive understanding of the behaviour and fate of Sb isotopes. However, there is still some challenges regarding the wide application of Sb isotopes to trace its sources and transport processes. The overlapping of several processes with similar (or opposite) fractionation factors can hinder their discrimination. More experimental studies are required to better characterise the behavior of Sb isotopes during complex geochemical processes and multi-source environments. While antimony extraction and environmental emissions are expected to increase in the near future (Zhou et al., 2015), the development of this understudied Sb isotopic system could ultimately lead to better identification of Sb sources in the environment when multiple contamination sources (mining, industrial and/or urban sources) co-exist, which is essential for implementing effective emission reduction strategies.

Acknowledgments

This work received financial support from the CNRS INSU EC2CO program (Project AntiBol). We thank Sophie Delpoux and Léa Causse for the speciation and trace element analysis performed on the AETE-ISO platform, OSU OREME/Université de Montpellier. All the IRD office in Bolivia is thanked for its logistical support in Bolivia and in particular Abdul Castillo and Julio César Salinas for their assistance in the field.

Statements and Declarations

The authors declare no known conflict of interest in the submission of this manuscript.

Research Data Policy and Data Availability Statements

The authors declare that the data supporting the findings of this study are available within the paper, its supplementary information files, and will be made available on request.

Credit authorship contribution statement

C. Ferrari: Investigation, Formal analysis, Visualization, Writing - Original Draft, Writing - Review & Editing. **E. Resongles:** Conceptualization, Methodology, Investigation, Formal analysis, Visualization, Writing - Original Draft, Writing - Review & Editing, Supervision. **R. Freydier:** Investigation, Writing - Review & Editing, Supervision. **M. Flores:** Investigation, Writing - Review & Editing. **M. Ormachea:** Investigation, Resources, Writing - Review & Editing. **G. Zamora:** Investigation, Resources, Writing - Review & Editing. **C. Casiot:** Conceptualization, Methodology, Investigation, Formal analysis, Writing - Original Draft, Writing - Review & Editing, Project administration, Supervision, Funding acquisition.

References

Barbieri, F.L. *et al.* (2011) 'Hair Trace Elements Concentration to Describe Polymetallic Mining Waste Exposure in Bolivian Altiplano', *Biological Trace Element Research*, 139(1), pp. 10–23. https://doi.org/10.1007/s12011-010-8641-1.

Barbieri, E. *et al.* (2014) 'Indoor metallic pollution and children exposure in a mining city', *Science of The Total Environment*, 487, pp. 13–19. https://doi.org/10.1016/j.scitotenv.2014.03.136.

Barbieri, F.L. *et al.* (2016) 'Toxic trace elements in maternal and cord blood and social determinants in a Bolivian mining city', *International Journal of Environmental Health Research*, 26(2), pp. 158–174. https://doi.org/10.1080/09603123.2015.1061114.

Bigham, J.M. *et al.* (1996) 'Schwertmannite and the chemical modeling of iron in acid sulfate waters', *Geochimica et Cosmochimica Acta*, 60(12), pp. 2111–2121. https://doi.org/10.1016/0016-7037(96)00091-9.

Bolan, N. *et al.* (2022) 'Antimony contamination and its risk management in complex environmental settings: A review', *Environment International*, 158, p. 106908. https://doi.org/10.1016/j.envint.2021.106908.

Cavallo, D. *et al.* (2002) 'Genotoxic risk and oxidative DNA damage in workers exposed to antimony trioxide', *Environmental and Molecular Mutagenesis*, 40(3), pp. 184–189. https://doi.org/10.1002/em.10102.

Chang, T.-L. *et al.* (1993) 'The isotopic abundance of antimony', *International Journal of Mass Spectrometry and Ion Processes*, 123(1), pp. 77–82. https://doi.org/10.1016/0168-1176(93)87056-X.

Chen, H. *et al.* (2023) 'In-situ immobilization of arsenic and antimony containing acid mine drainage through chemically forming layered double hydroxides', *Science of The Total Environment*, 903, p. 166601. https://doi.org/10.1016/j.scitotenv.2023.166601.

Daus, B. and Wennrich, R. (2014) 'Investigation on stability and preservation of antimonite in iron rich water samples', *Analytica Chimica Acta*, 847, pp. 44–48. https://doi.org/10.1016/j.aca.2014.08.019.

Degryse, P. *et al.* (2020) 'Isotopic evidence for the use of Caucasian antimony in Late Bronze Age glass making', *Journal of Archaeological Science*, 120, p. 105195. https://doi.org/10.1016/j.jas.2020.105195.

Dembele, S., Akcil, A. and Panda, S. (2022) 'Technological trends, emerging applications and metallurgical strategies in antimony recovery from stibnite', *Minerals Engineering*, 175, p. 107304. https://doi.org/10.1016/j.mineng.2021.107304.

Ferrari, C *et al.,* (2021) 'A single-step purification method for the precise determination of the antimony isotopic composition of environmental, geological and biological samples by HG-MC-ICP-MS', *Journal of Analytical Atomic Spectrometry*, 36(11), pp. 2560–2560. https://doi.org/10.1039/D1JA90048J.

Ferrari, C. *et al.* (2022) 'Equilibrium mass-dependent isotope fractionation of antimony between stibnite and Sb secondary minerals: A first-principles study', *Chemical Geology*, p. 121115. https://doi.org/10.1016/j.chemgeo.2022.121115.

Ferrari, C. *et al.* (2023) 'Antimony isotopic fractionation during Sb(III) oxidation to Sb(V): Biotic and abiotic processes', *Chemical Geology*, p. 121788. https://doi.org/10.1016/j.chemgeo.2023.121788.

Ferrari, C. *et al.* (2024) 'Antimony isotope fractionation during Sb(V) and Sb(III) adsorption on secondary Fe-minerals (schwertmannite, ferrihydrite) typical of mine waters', *Applied Geochemistry.* https://doi.org/10.1016/j.apgeochem.2024.105935

Filella, M., Belzile, N. and Chen, Y.-W. (2001) 'Antimony in the environment: a review focused on natural waters. I. Occurence', *Earth-Sciences Reviews*, 57, pp. 125–176. https://doi.org/10.1016/S0012-8252(01)00070-8.

Filella, M. *et al.* (2009) 'Natural attenuation processes applying to antimony: A study in the abandoned antimony mine in Goesdorf, Luxembourg', *Science of The Total Environment*, 407(24), pp. 6205–6216. https://doi.org/10.1016/j.scitotenv.2009.08.027.

Fort, M. *et al.* (2016) 'Evaluation of atmospheric inputs as possible sources of antimony in pregnant women from urban areas', *Science of The Total Environment*, 544, pp. 391–399. https://doi.org/10.1016/j.scitotenv.2015.11.095.

Fu, X. *et al.* (2023) 'A review on distribution, biogeochemistry of antimony in water and its environmental risk', *Journal of Hydrology*, 625, p. 130043. https://doi.org/10.1016/j.jhydrol.2023.130043.

Fukushi, K. *et al.* (2003) 'A natural attenuation of arsenic in drainage from an abandoned arsenic mine dump', *Applied Geochemistry*, 18(8), pp. 1267–1278. https://doi.org/10.1016/S0883-2927(03)00011-8.

693 Gao, B. *et al.* (2013) 'Cd isotopes as a potential source tracer of metal pollution in river sediments',
694 *Environmental Pollution*, 181, pp. 340–343. https://doi.org/10.1016/j.envpol.2013.05.048.

695 Goix, S. (2012) *Origine et impact des pollutions liées aux activités minières sur l'environnement et la*
696 *santé, cas de Oruro (Bolivie)*. PhD dissertation, Université de Toulouse. Available at:
697 https://tel.archives-ouvertes.fr/tel-00781152/file/Goix_these.pdf.

698 Goix, S. *et al.* (2013) 'Transplantation of epiphytic bioaccumulators (Tillandsia capillaris) for high spatial
699 resolution biomonitoring of trace elements and point sources deconvolution in a complex
700 mining/smelting urban context', *Atmospheric Environment*, 80, pp. 330–341.
701 https://doi.org/10.1016/j.atmosenv.2013.08.011.

702 Goix, S. *et al.* (2016) 'Metal concentration and bioaccessibility in different particle sizes of dust and
703 aerosols to refine metal exposure assessment', *Journal of Hazardous Materials*, 317, pp. 552–562.
704 https://doi.org/10.1016/j.jhazmat.2016.05.083.

705 Gómez, *et al.* (2016). Groundwater origins and circulation patterns based on isotopes in Challapampa
706 aquifer, Bolivia. *Water*, *8*(5), 207. https://doi.org/10.3390/w8050207

707 Gómez, *et al.* (2019). Alluvial aquifer thickness and bedrock structure delineation by electromagnetic
708 methods in the highlands of Bolivia. *Environmental Earth Sciences*, *78*, 1-13.
709 https://doi.org/10.1007/s12665-019-8074-x

710 Guillevic, F. *et al.* (2024) 'Multi-isotope (Pb, Sb) approach to trace metallic contaminant sources at a
711 historical mining and metallurgical site', *Chemical Geology*, p. 121958.
712 https://doi.org/10.1016/j.chemgeo.2024.121958.

713 Guo, J. *et al.* (2016) 'Relationships between urinary antimony levels and both mortalities and
714 prevalence of cancers and heart diseases in general US population, NHANES 1999–2010', *Science of*
715 *The Total Environment*, 571, pp. 452–460. https://doi.org/10.1016/j.scitotenv.2016.07.011.

716 Guo, W. *et al.* (2018) 'Environmental geochemical and spatial/temporal behavior of total and
717 speciation of antimony in typical contaminated aquatic environment from Xikuangshan, China',
718 *Microchemical Journal*, 137, pp. 181–189. https://doi.org/10.1016/j.microc.2017.10.010.

719 Hao, C. *et al.* (2021) 'Contrasting water–rock interaction behaviors of antimony and arsenic in
720 contaminated rivers around an antimony mine, Hunan Province, China', *Geochemistry*, 81(2), p.
721 125748. https://doi.org/10.1016/j.chemer.2021.125748.

722 He, M. *et al.* (2019) 'Antimony speciation in the environment: Recent advances in understanding the
723 biogeochemical processes and ecological effects', *Journal of Environmental Sciences*, 75, pp. 14–39.
724 https://doi.org/10.1016/j.jes.2018.05.023.

725 Hiller, E. *et al.* (2012) 'Arsenic and antimony contamination of waters, stream sediments and soils in
726 the vicinity of abandoned antimony mines in the Western Carpathians, Slovakia', *Applied*
727 *Geochemistry*, 27(3), pp. 598–614. https://doi.org/10.1016/j.apgeochem.2011.12.005.

728 Jia, X., *et al.* (2024) 'Antimony Isotope Fractionation during Kinetic Sb (III) Oxidation by Antimony-
729 Oxidizing Bacteria Pseudomonas sp. J1.' *Environmental Science & Technology* 58(26), pp. 11411-11420.
730 https://doi.org/10.1021/acs.est.3c10271

731 Kaufmann, A.B. *et al.* (2023) 'Changes in antimony isotopic composition as a tracer of hydrothermal
732 fluid evolution at the Sb deposits in Pezinok (Slovakia)', *Mineralium Deposit,* pp. 1-17.
733 https://doi.org/10.1007/s00126-023-01222-7.

734 Kaufmann, Andreas B., et al. (2024) "Weathering-induced Sb isotope fractionation during leaching of
735 stibnite and formation of secondary Sb minerals." *Chemical Geology* 662, p. 122253.
736 https://doi.org/10.1016/j.chemgeo.2024.122253

Keutsch, F. and Brodtkorb, M.K. de (2008) 'Metalliferous paragenesis of the San José mine, Oruro, Bolivia', *Journal of South American Earth Sciences*, 25(4), pp. 485–491. https://doi.org/10.1016/j.jsames.2007.12.003.

Li, C. *et al.* (2020) 'High Antimony Source and Geochemical Behaviors in Mine Drainage Water in China's Largest Antimony Mine', *Polish Journal of Environmental Studies*, 29(5), pp. 3663–3673. https://doi.org/10.15244/pjoes/114970.

Liao, J. *et al.* (2023) 'Antimony isotope fractionation and the key controls in the soil profiles of an antimony smelting area', *Journal of Hazardous Materials*, 454, p. 131553. https://doi.org/10.1016/j.jhazmat.2023.131553.

Liu, Huiji, et al. (2024) 'The composition and differences of antimony isotopic in sediments affected by the world's largest antimony deposit zone.' *Water Research* 254, p.121427. https://doi.org/10.1016/j.watres.2024.121427.

Long, Z.-Y. *et al.* (2022) 'Fingerprinting the metal source and cycling of the world's largest antimony deposit in Xikuangshan, China', *GSA Bulletin,* 135, pp. 286-294 . https://doi.org/10.1130/B36377.1.

Luo, J., et al. (2024) 'Antimony Isotope Fractionation during Adsorption on Iron (Oxyhydr) oxides." *Environmental Science & Technology* 58, pp. 695-703. https://doi.org/10.1021/acs.est.3c05867.

Manaka, M. *et al.* (2007) 'Natural attenuation of antimony in mine drainage water', *Geochemical Journal*, 41(1), pp. 17–27. https://doi.org/10.2343/geochemj.41.17.

Novak, M. *et al.* (2017). Chromium isotope fractionations resulting from electroplating, chromating and anodizing: Implications for groundwater pollution studies. *Applied geochemistry*, 80, pp. 134-142. https://doi.org/10.1016/j.apgeochem.2017.03.009

Philippe, M. *et al.* (2023) 'Fate of antimony contamination generated by road traffic – A focus on Sb geochemistry and speciation in stormwater ponds', *Chemosphere*, 313, p. 137368. https://doi.org/10.1016/j.chemosphere.2022.137368.

Resongles, E. *et al.* (2013) 'Fate of Sb(V) and Sb(III) species along a gradient of pH and oxygen concentration in the Canoulès mine waters (Southern France)', *Environmental Science Processes and Impacts*, 15, pp. 1536–1544. https://doi.org/10.1039/c3em00215b.

Resongles, E. *et al.* (2015) 'Antimony isotopic composition in river waters affected by ancient mining activity', *Talanta*, 144, pp. 851–861. http://dx.doi.org/10.1016/j.talanta.2015.07.013.

Ritchie, V.J. *et al.* (2013) 'Mobility and chemical fate of antimony and arsenic in historic mining environments of the Kantishna Hills district, Denali National Park and Preserve, Alaska', *Chemical Geology*, 335, pp. 172–188. https://doi.org/10.1016/j.chemgeo.2012.10.016.

Rouxel, O., Ludden, J. and Fouquet, Y. (2003) 'Antimony isotope variations in natural systems and implications for their use as geochemical tracers', *Chemical Geology*, 200, pp. 25–40. https://doi.org/10.1016/S0009-2541(03)00121-9.

Saerens, A. *et al.* (2019) 'Risk of Cancer for Workers Exposed to Antimony Compounds: A Systematic Review', *International Journal of Environmental Research and Public Health*, 16(22), p. 4474. https://doi.org/10.3390/ijerph16224474.

SELA, Servicio Local de acueductos y alcantarillado – Oruro, Informe Anual 2023. Available at: https://selaoruro.gob.bo.

Sivry, Y. *et al.* (2008) 'Zn isotopes as tracers of anthropogenic pollution from Zn-ore smelters The Riou Mort–Lot River system', *Chemical Geology*, 255(3), pp. 295–304. https://doi.org/10.1016/j.chemgeo.2008.06.038.

780 Slejko, F. *et al.* 2019). Chromium isotopes tracking the resurgence of hexavalent chromium
781 contamination in a past-contaminated area in the Friuli Venezia Giulia Region, northern Italy. *Isotopes*
782 *in Environmental and Health Studies*, 55(1), pp. 56–69.
783 https://doi.org/10.1080/10256016.2018.1560278

784 Sonke, J.E. *et al.* (2008) 'Historical variations in the isotopic composition of atmospheric zinc deposition
785 from a zinc smelter', *Chemical Geology*, 252(3), pp. 145–157.
786 https://doi.org/10.1016/j.chemgeo.2008.02.006.

787 Sundar, S. and Chakravarty (2010) 'Antimony Toxicity', *International Journal of Environmental Research*
788 *and Public Health*, 7, pp. 4267–4277. https://doi.org/10.3390/ijerph7124267.

789 U.S.G.S (2023) *Mineral commodity summaries 2023*, *Mineral Commodity Summaries*. 2023. U.S.
790 Geological Survey. https://doi.org/10.3133/mcs2023.

791 Tanimizu, M. *et al.* (2011) 'Determination of natural isotopic variation in antimony using inductively
792 coupled plasma mass spectrometry for an uncertainty estimation of the standard atomic weight of
793 antimony', *Geochemical Journal*, 45, pp. 27–32. https://doi.org/10.2343/geochemj.1.0088.

794 Tapia, J. *et al.* (2012) 'Geochemical background, baseline and origin of contaminants from sediments
795 in the mining-impacted Altiplano and Eastern Cordillera of Oruro, Bolivia', *Geochemistry: Exploration,*
796 *Environment, Analysis*, 12(1), pp. 3–20. https://doi.org/10.1144/1467-7873/10-RA-049.

797 Veldhuizen, H.J., MacKinney, J.S. and Johnson, T.M. (2023) 'Kinetic Fractionation of Antimony Isotopes
798 during Reduction by Sulfide', *ACS Earth and Space Chemistry*, 7(12), pp. 2603–2612.
799 https://doi.org/10.1021/acsearthspacechem.3c00269.

800 Wang, X. *et al.* (2011) 'Antimony distribution and mobility in rivers around the world's largest antimony
801 mine of Xikuangshan, Hunan Province, China', *Microchemical Journal*, 97(1), pp. 4–11.
802 https://doi.org/10.1016/j.microc.2010.05.011.

803 Wang, D. *et al.* (2021) 'Redox-controlled antimony isotope fractionation in the epithermal system: New
804 insights from a multiple metal stable isotopic combination study of the Zhaxikang Sb–Pb–Zn–Ag
805 deposit in Southern Tibet', *Chemical Geology*, 584, p. 120541.
806 https://doi.org/10.1016/j.chemgeo.2021.120541.

807 Wen, B. *et al.* (2023) 'Antimony (Sb) isotopic signature in water systems from the world's largest Sb
808 mine, central China: Novel insights to trace Sb source and mobilization', *Journal of Hazardous*
809 *Materials*, 446, p. 130622. https://doi.org/10.1016/j.jhazmat.2022.130622.

810 Wen, B., et al. (2024) 'Antimony isotopic fractionation induced by Sb (V) adsorption on β-MnO2.'
811 *Science of The Total Environment* 933, pp. 172972. https://doi.org/10.1016/j.scitotenv.2024.172972

812 Wiederhold, J.G. (2015) 'Metal Stable Isotope Signatures as Tracers in Environmental Geochemistry',
813 *Environmental Science & Technology*, 49(5), pp. 2606–2624. https://doi.org/10.1021/es504683e.

814 Wilson, N.J., Craw, D. and Hunter, K. (2004) 'Antimony distribution and environmental mobility at an
815 historic antimony smelter site, New Zealand', *Environmental Pollution*, 129(2), pp. 257–266.
816 https://doi.org/10.1016/j.envpol.2003.10.014.

817 Wu, D. and Pichler, T. (2016) 'Preservation of co-occurring As, Sb and Se species in water samples with
818 EDTA and acidification', *Geochemistry: Exploration, Environment, Analysis*, 16(2), pp. 117–125.
819 https://doi.org/10.1144/geochem2015-369

820 Wu, Y. *et al.* (2024). Antimony isotopic fractionation during intensive chemical weathering of basalt in
821 the tropics. *Geochimica et Cosmochimica Acta*, *367*, 29-40. https://doi.org/10.1016/j.gca.2023.12.029.

Wu, Y. *et al.* (2025). 'Identification of the sources and migration of antimony in karst terraces via Sb stable isotopes.' *Journal of Hazardous Materials*, p. 138570. https://doi.org/10.1016/j.jhazmat.2025.138570.

Ye, L. *et al.* (2018) 'Antimony exposure and speciation in human biomarkers near an active mining area in Hunan, China', *Science of The Total Environment*, 640–641, pp. 1–8. https://doi.org/10.1016/j.scitotenv.2018.05.267.

Zhai, D. *et al.* (2021) 'Antimony isotope fractionation in hydrothermal systems', *Geochimica et Cosmochimica Acta*, 306, pp. 84-97. https://doi.org/10.1016/j.gca.2021.05.031.

Zhou, J. *et al.* (2015) 'Future trends of global atmospheric antimony emissions from anthropogenic activities until 2050', *Atmospheric Environment*, 120, 385-392.

Zhou, J. *et al.* (2017) 'Mine waste acidic potential and distribution of antimony and arsenic in waters of the Xikuangshan mine, China', *Applied Geochemistry*, 77, pp. 52–61. https://doi.org/10.1016/j.apgeochem.2016.04.010.

Zhou, W. *et al.* (2022) 'Antimony isotope fractionation during adsorption on aluminum oxides', *Journal of Hazardous Materials*, 429, p. 128317. https://doi.org/10.1016/j.jhazmat.2022.128317.

Zhou, W. *et al.* (2023) 'Antimony Isotope Fractionation Revealed from EXAFS during Adsorption on Fe (Oxyhydr)oxides', *Environmental Science & Technology*, 57(25), pp. 9353–9361. https://doi.org/10.1021/acs.est.3c01906.

Zhou, Z., et al. (2024) 'Antimony stable isotope fractionation during adsorption onto birnessite: A molecular perspective from X-ray absorption spectroscopy and density functional theory.' *Geochimica et Cosmochimica Acta* 386, p. 173-184. https://doi.org/10.1016/j.gca.2024.09.028